Article

Neuron

Single-Cell mRNA Profiling Reveals Cell-Type-Specific Expression of Neurexin Isoforms

Highlights

- Single-cell neurexin transcriptional repertoires display cell-type specificity
- Neurexin expression in individual neurons is coordinated in a region-specific manner
- Neurexin transcriptional profiles are plastic in response to a drug of abuse
- This study provides first evidence for a cell-type-specific synaptic adhesion code

Authors

Marc V. Fuccillo, Csaba Földy, Özgün Gökce, ..., Gordon L. Sun, Robert C. Malenka, Thomas C. Südhof

Correspondence

fuccillo@mail.med.upenn.edu (M.V.F.), tcs1@stanford.edu (T.C.S.)

In Brief

The diversity of synaptic adhesion molecules, and neurexins in particular, may provide a molecular substrate for the formation of neural circuits. Using single-cell qPCR, Fuccillo et al. demonstrate that individual neurons exhibit unique and reproducible cell-type-specific neurexin mRNA repertoires.

Fuccillo et al., 2015, Neuron *87*, 326–340
July 15, 2015
http://dx.doi.org/10.1016/j.neuron.2015.06.028

CellPress

CellPress

Neuron
Article

Single-Cell mRNA Profiling Reveals Cell-Type-Specific Expression of Neurexin Isoforms

Marc V. Fuccillo,[1,2,4,5,*] Csaba Földy,[1,2,4] Özgün Gökce,[1,4] Patrick E. Rothwell,[1,2] Gordon L. Sun,[2] Robert C. Malenka,[2] and Thomas C. Südhof[1,3,*]

[1]Department of Molecular and Cellular Physiology
[2]Nancy Pritzker Laboratory, Department of Psychiatry and Behavioral Sciences
[3]Howard Hughes Medical Institute
School of Medicine, Stanford University, Stanford, CA 94305, USA
[4]Co-first author
[5]Present address: Department of Neuroscience, Perelman School of Medicine, University of Pennsylvania, Philadelphia, PA 19104, USA
*Correspondence: fuccillo@mail.med.upenn.edu (M.V.F.), tcs1@stanford.edu (T.C.S.)
http://dx.doi.org/10.1016/j.neuron.2015.06.028

SUMMARY

Neurexins are considered central organizers of synapse architecture that are implicated in neuropsychiatric disorders. Expression of neurexins in hundreds of alternatively spliced isoforms suggested that individual neurons might exhibit a cell-type-specific neurexin expression pattern (a neurexin code). To test this hypothesis, we quantified the single-cell levels of neurexin isoforms and other *trans*-synaptic cell-adhesion molecules by microfluidics-based RT-PCR. We show that the neurexin repertoire displays pronounced cell-type specificity that is remarkably consistent within each type of neuron. Furthermore, we uncovered region-specific regulation of neurexin transcription and splice-site usage. Finally, we demonstrate that the transcriptional profiles of neurexins can be altered in an experience-dependent fashion by exposure to a drug of abuse. Our data provide evidence of cell-type-specific expression patterns of multiple neurexins at the single-cell level and suggest that expression of synaptic cell-adhesion molecules overlaps with other key features of cellular identity and diversity.

INTRODUCTION

Normal brain function relies on the precise development of neuronal circuits—specific cellular ensembles that exhibit stereotyped patterns of connectivity and synaptic functionality (Klausberger and Somogyi, 2008). This organization requires exquisitely orchestrated developmental programs linking neuronal cell-type specification to the targeting and formation of synapses with unique functional characteristics (Duan et al., 2014). The neurexin family of synaptic adhesion molecules, which are extensively linked to neuropsychiatric disease, has been proposed to organize synaptic function throughout the nervous system (Missler et al., 2003; Südhof, 2008). The large genomic footprint of the three neurexin molecules exhibits astounding complexity, including alternative promoter usage, extensive splice-site regulation, and large intronic segments (Tabuchi and Südhof, 2002). The extensive transcriptional diversity generated from these genes makes it possible that neurexin proteins serve as molecular backbones supporting multiple *trans*-synaptic interactions in individual synapses, which have unique properties throughout the brain. A central implication of this hypothesis is that neurexin mRNA expression should be tightly regulated and unique to each cell type in the circuit—a premise that we directly test here by using single-cell analysis of neurexin transcriptional and splice-site isoforms as well as those of other families of synaptic cell-adhesion molecule.

Neurexin protein diversity is achieved through transcriptional and post-transcriptional regulation (Ushkaryov et al., 1992; Ullrich et al., 1995). All neurexin genes (*Nrxn1-Nrxn3* in mice, *NRXN1-NRXN3* in humans) use two promoters that generate long (α) and short (β) transcripts (Tabuchi and Südhof, 2002; Ushkaryov et al., 1992; Ushkaryov and Südhof, 1993). In addition, six canonical sites of alternative splicing in α-neurexins and two such sites in β-neurexins, if utilized independently, potentially generate thousands of distinct isoforms (Ullrich et al., 1995), a hypothesis that was confirmed by recent studies using long, single-molecule sequencing (Treutlein et al., 2014; Schreiner et al., 2014). Crystal structures of Nrxn1α and Nrxn1β have revealed that alignment of their domains creates multiple binding pockets capable of interacting with several proteins, thereby mediating neurexin's function as a synaptic "hub" molecule (Araç et al., 2007; Chen et al., 2010, 2011; Comoletti et al., 2010). The alternatively spliced sequences often line these binding pockets, thus modulating neurexin-binding activities. These data suggest that, through regulation of neurexin mRNA expression and alternative splicing, neurons modulate binding to a series of *trans*-synaptic partners to sculpt synaptic connectivity and function (Aoto et al., 2013; Boucard et al., 2005; Siddiqui et al., 2010; Soler-Llavina et al., 2011, 2013; Treutlein et al., 2014). To date, the diversity of neurexin mRNA expression has

been explored by in situ hybridization as well as by global analysis of mRNA isolated from dissected tissue, using both direct sequencing and qRT-PCR (Ullrich et al., 1995; Aoto et al., 2013; Treutlein et al., 2014; Schreiner et al., 2014). However, while current single-molecule, deep-sequencing approaches have identified predominant neurexin mRNA species, they lacked cellular resolution and do not reveal the expression of specific neurexin isoforms in particular types of neurons.

The role for neurexins in regulating synaptic diversity of microcircuits likely takes place on a cell-by-cell basis, therefore requiring techniques that assess mRNA expression of individual neurons to fully understand the role of neurexins in circuit formation and function. At single-cell resolution, the unanswered questions are numerous: for instance, is neurexin diversity manifest at the single-cell level, and, if so, what are the relative contributions of transcriptional regulation and alternative splicing? Are neurexin transcription profiles common within specific circuits, or does each functional unit have unique transcript patterns? How is neurexin expression related to that of other pre- and postsynaptic adhesion modules? Finally, are cellular neurexin transcription profiles static, or can they be remodeled by behavioral experience? The present study leverages current advances in single-cell transcription profiling with genetic tools for circuit dissection to examine the diversity of synaptic cell-adhesion molecule expression and to assess how such diversity relates to specific cell types and patterns of connectivity. We find that neurexin transcriptional repertoires are cell type specific but are not related to particular synaptic connectivity. Furthermore, neurexins display a brain-region-specific coordination of alternative splicing at the single-cell level. Finally, we demonstrate that neurexin expression profiles are plastic, in that they can be altered by exposure to drugs of abuse.

RESULTS

Single-Cell Neurexin Expression Profiles Are Distinct from Those Observed in Tissue Samples

Our characterization of neurexin expression profiles of select neuronal circuits relied upon two methodologies: first, BAC (bacterial artificial chromosome) transgenic mice or rabies-virus (RV)-mediated retrograde tracing to select neurons that are constituents of a particular circuit by cell type or patterns of connectivity; second, the design and characterization of a library of qPCR assays that could specifically detect splice isoforms of neurexin transcripts. Using a Fluidigm microfluidics platform, we tested over 150 probes on cytosol of single neurons aspirated through a patch pipette from acute slices (Figure 1A). Probe-based qPCR assays were constructed to investigate a substantial fraction of the numerous neurexin splice sites (Figure 1B). Splice-site-specific primers were designed to detect omission of an intervening exon, designated as splice site out (ss-OUT), or inclusion of an intervening exon, designated as splice site in (ss-IN) (Figure 1C). The amplification efficiency (Figure 1D) and specificity (Figure 1E) of all probes were tested on tissue mRNA from multiple brain regions as well as plasmids containing specific splice isoforms. Using this strategy, we were able to generate a primer library encompassing the majority of potential neurexin mRNA variants, including specific splice isoforms and the two major transcriptional species for each neurexin gene (see Table S1 for primer info).

To date, analysis of neurexin expression diversity has been performed exclusively on mRNA extracted from neuronal tissue and cultured neurons, potentially masking cell-type- and circuit-specific differences (Ullrich et al., 1995; Aoto et al., 2013; Treutlein et al., 2014; Schreiner et al., 2014;). To reliably uncover patterns of neurexin mRNA expression at the single-neuron level, it is essential to minimize the experimental variability introduced by inconsistencies in qPCR detection or cytosolic input material. Replication experiments on a subset of single-cell cDNA samples demonstrated a nearly linear fit between qPCR runs, suggesting that microfluidics-based transcript detection is reliable from trial to trial (Figure 1F). Furthermore, initial cytosolic mRNA input was largely consistent across single cells, as judged by average cycle threshold (Ct) values for three housekeeping probes used in subsequent normalization steps (Figure 1G). To test whether our approach can differentiate neurexin expression at the single-cell level from that of the surrounding tissue, we compared the transcriptional profiles of the α- and β-variants of Nrxn1, Nrxn2, and Nrxn3 from micro-dissected hippocampal CA1 tissue with single cells from the CA1 pyramidal layer or isolated putative cholecystokinin-positive (CCK+) interneurons within the stratum radiatum (Figure 1H). Single-cell mRNA extraction by somatic patch-pipette aspiration consistently reduced the level of detected glial transcripts, which are expectedly present in tissue samples (Figure S1). Consistent with the preponderance of pyramidal cells in the CA1 field, tissue expression values of neurexins were similar to averaged single CA1 pyramidal cell expression levels (Figure 1H). In contrast, tissue expression levels clearly diverged from those of averaged putative CCK cells, a subclass of interneuron far less numerous than hippocampal pyramidal cells (Figure 1H). Perhaps due to its GC-rich sequence content, we were unable to reliably detect Nrxn2 isoforms both from tissue samples and from single cells, prompting us to omit Nrxn2 from the remaining analyses (Figure 1H). Overall, these data suggest that single-neuron neurexin transcriptional analysis is feasible and robust and can provide novel insights into the cellular regulation of synaptic cell-adhesion networks.

Neurexin Expression Repertoires Exhibit Pronounced Cell-Type Specificity across Multiple Microcircuits

Our initial data suggest that CCK interneurons display neurexin transcriptional profiles that are distinct from surrounding CA1 pyramidal cells. To determine whether this transcriptional diversity is shared by other local circuit GABAergic interneurons in the stratum radiatum, we targeted another well-defined cell population for mRNA profiling: parvalbumin-positive (PV+) interneurons, which share postsynaptic targets with CCK cells but display highly divergent synaptic properties (Freund and Katona, 2007). PV-Cre mice were crossed with AI9 reporter mice to label the PV+ subclass, and the cytosol of fluorescent cells in close proximity to the CA1 hippocampal pyramidal cell layer was aspirated from acute hippocampal slices (Figure 2A) (Hippenmeyer et al., 2007; Madisen et al., 2010). We identified CCK+ cells based on their soma location—similar to that of PV+ cells—their larger soma sizes, and absence of red fluorescence. While none of these characteristics are alone sufficient to identify these cell

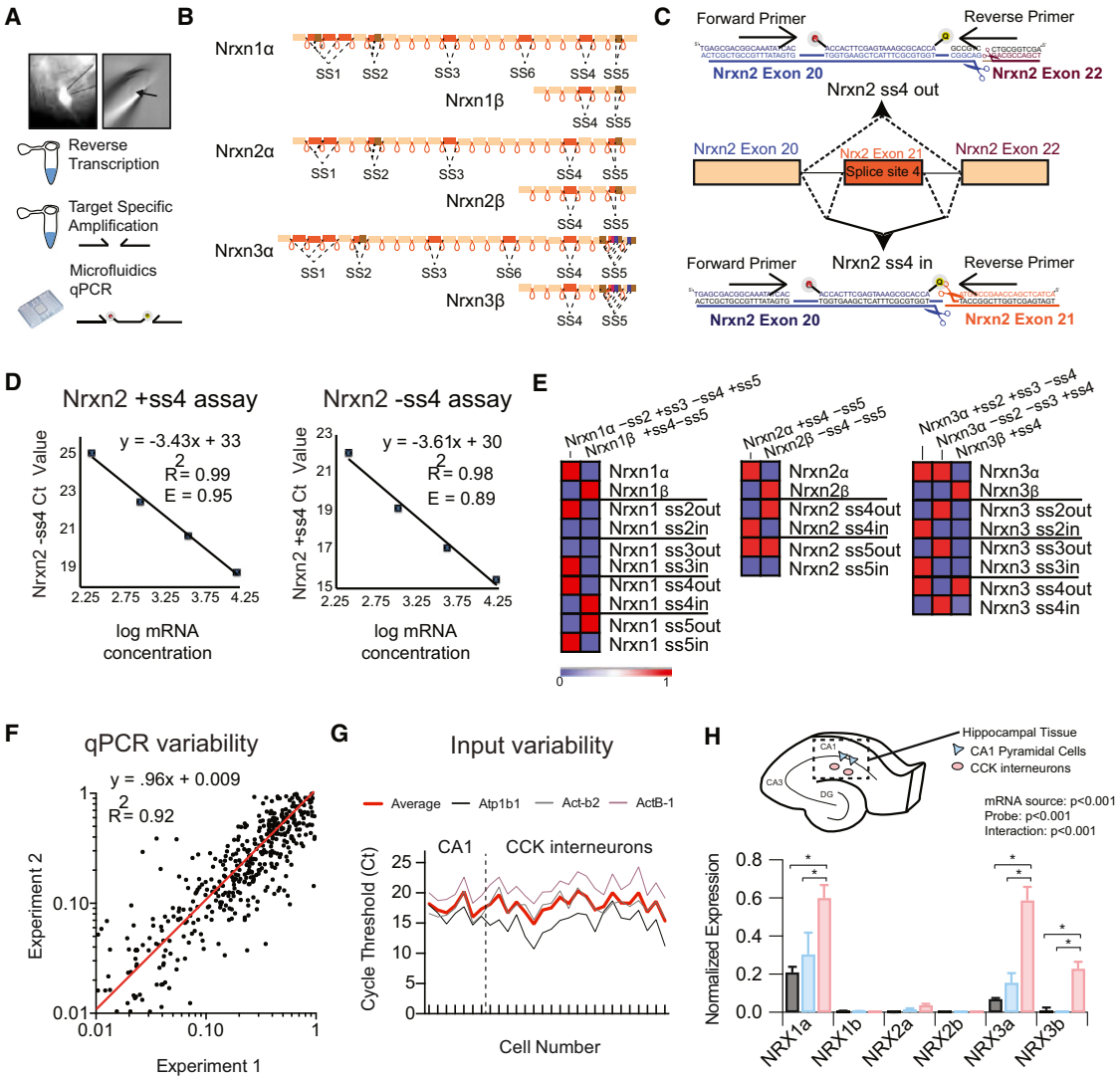

Figure 1. Single-Cell Neurexin Transcriptional Profiles Are Distinct from Those Observed in Tissue Samples

(A) Left: image of 40× fluorescent field showing pipette extraction (solid outline) of GFP-positive cell (dotted outline) from adult striatum. Right: cellular contents and nucleus (arrow) within the extraction pipette. Bottom: General workflow from single-cell extraction to target-specific amplification of reverse-transcribed cDNA.

(B) Schematic depicting the genomic architecture of Nrxn1–3.

(C) An example strategy for the design of Nrxn2 ss4-specific primers is shown, which uses common forward primer and internal probe with unique reverse primer to differentiate inclusion or skipping of exon 21.

(D) Primer efficiency determination through plotting of Ct versus mRNA concentration in serial dilution.

(E) Heatmap representation of Ct for plasmid DNA with known splice-site content.

(F) Measurement of trial-to-trial qPCR variability (experiment 1 versus experiment 2) for all probes across single-cell cDNAs (n = 24) demonstrates a near-linear fit (red line).

(G) Assessment of input variability for CA1 pyramidal cells and CCK+ interneurons by plotting of Ct for three normalization probes across all collected single cells (red indicates a three-probe average).

(H) Top: schematic depicting mRNA isolation from hippocampal CA1 field for transcriptional analysis of hippocampal tissue (n = 6) and individual CA1 pyramidal cells (n = 7) or stratum radiatum CCK interneurons (n = 22). Bottom: averaged normalized expression for the long and short neurexin transcriptional isoforms for hippocampal tissue and single-cell populations.

Data are means ± SEM. Asterisk indicates significant difference between groups (ANOVA), with Tukey's multiple comparison post hoc test.

types, our single-cell results demonstrated unique expression of markers previously associated with PV+ and CCK+ cells in this region (Figure 2B) (Földy et al., 2007; Freund, 2003). Despite having common pyramidal neuron targets, the neurexin transcriptional profiles of PV+ and CCK+ interneurons were highly distinct, with both Nrxn1α and Nrxn3α/β more abundantly expressed in CCK+ interneurons than in PV+ interneurons (Figures 2C and 2D).

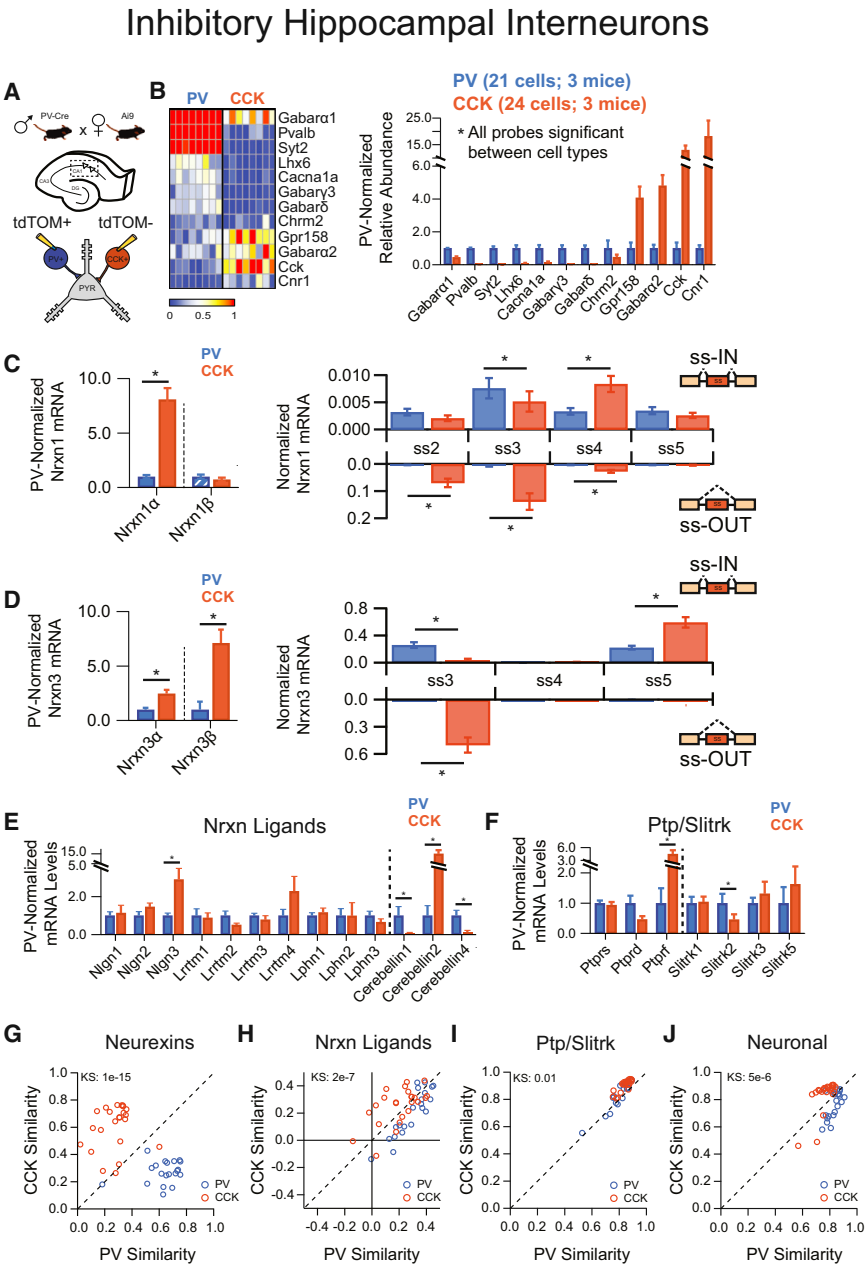

Figure 2. Hippocampal Interneurons Exhibit Cell-Type-Specific Neurexin Expression Patterns

(A) Illustration of the genetic cross used to label hippocampal interneurons for pipette extraction.

(B) Left: heatmap representation of normalized expression of PV+ and CCK+ interneurons for genes known to mark these subtypes. Right: averaged single-cell normalized expression for PV+ (n = 21) and CCK+ (n = 24).

(C and D) Left: Nrxn α/β isoform expression, normalized to the average level in PV+ cells (hatched PV bars designate expression value <1%). Right: splice-site graph showing averaged single-cell splice isoform expression values for ss-IN (upward bars) and ss-OUT (downward bars).

(E and F) Averaged single-cell normalized expression values for neurexin ligands (E, dotted line separates putative postsynaptic and secreted protein products) and the Ptp/Slitrk family (F, dotted line separates receptors from putative postsynaptic ligands).

(G–J) Pearson coefficient correlation plots demonstrating the similarity of individual neurons to the two cell classes being compared for neurexin (G), neurexin ligands (H), the Ptp/Slitrk family (I), and general neuronal transcripts (J). Cells are color coded according to their known genetic identity. The dashed unity line represents cells that are equally similar to both cell types. Kolmogorov-Smirnov (KS) values are given for comparison of single-cell groups.

Data are means ± SEM. Asterisk indicates significant difference between groups (Mann-Whitney U test).

Beyond the cell-type-specific regulation of neurexin expression, further analysis revealed several instances of inverse splicing patterns between the two cell types—particularly for the third splice site (ss3) of Nrxn1 and Nrxn3 (Figures 2C and 2D, right panels). To explore how other synaptic adhesion molecules were regulated compared with neurexin mRNAs, we analyzed the single-cell expression of known neurexin ligands, of the protein tyrosine phosphatase receptors, and of Slitrk family proteins, all of which are proposed to participate in synaptic organizing complexes (Figures 2E and 2F) (Boucard et al., 2014; de Wit et al., 2009; Linhoff et al., 2009; Takahashi and Craig, 2013; Uemura et al., 2010; Yim et al., 2013). Similar to neurexin expression profiles, these synaptic adhesion molecules were differentially regulated between interneuron populations, as evidenced by differences in expression of Nlgn3, Cerebellins, Ptprs, and Slitrks.

To assess whether the expression profiles of neurexins were predictive of specific circuit constituents, we used Pearson coefficient measurements of neurexin expression covariance between all single cells. Applying this metric to our datasets clearly demonstrated that neurexin expression profiles could reliably separate interneuron populations (Figure 2G). To assess whether this was a unique property of neurexin molecules, we again applied correlation analysis to the same single-cell data, but instead using probe sets representing neurexin ligands, the Ptpr and Slitrk families, or more general neuronal transcripts (Figures 2H–2J; see Figure S4A for probe definitions). Probe sets for each class could sort single cells into two distinct populations (Figures 2H–2J), highlighting the extreme transcriptional diversity between interneuron populations with distinct properties (Tricoire et al., 2011).

Next, we tested whether cell-type-specific regulation of synaptic cell-adhesion molecules was a general principle. To do so, we sought another brain structure with similar overall

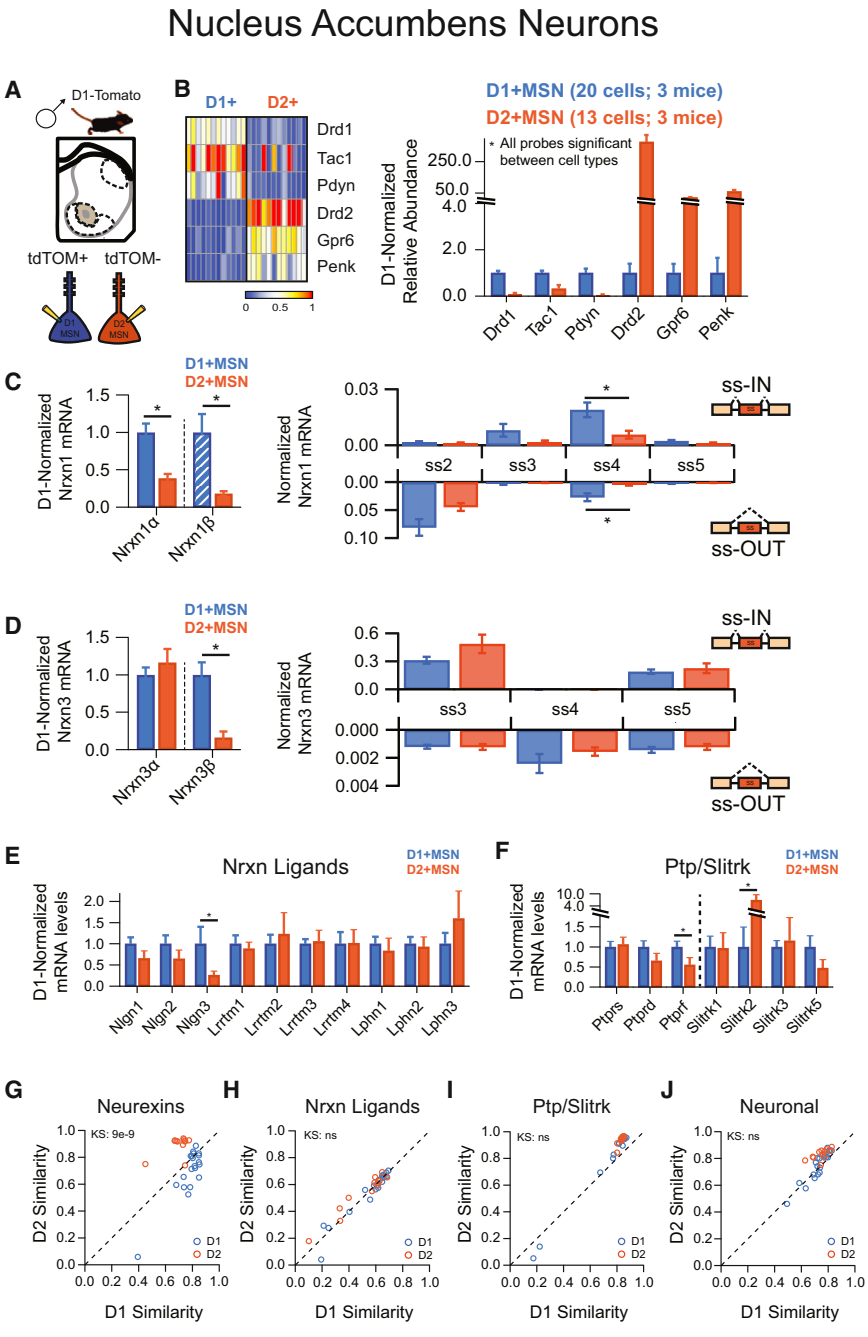

Figure 3. NAc MSNs Exhibit Cell-Type-Specific Neurexin Expression Patterns

(A) Illustration of picking strategy to isolate D1R+ and D2R+ MSN subtypes

(B) Left: heatmap representation of normalized expression of D1R+ and D2R+ MSNs for genes known to mark these subtypes. Right: averaged single-cell normalized expression for D1R+ (n = 20) and D2R+ (n = 13).

(C and D) Left: Nrxnα/β isoform expression, normalized to the average level in D1R+ cells (hatched D1+ MSN bars designate expression value <1%). Right: splice-site graph showing averaged single-cell splice isoform expression values for ss-IN (upward bars) and ss-OUT (downward bars).

(E and F) Averaged single-cell normalized expression values for neurexin ligands (E) and the Ptp/Slitrk family (F).

(G–J) Pearson coefficient correlation plots demonstrating the similarity of individual neurons to the two cell classes being compared for neurexins (G), neurexin ligands (H), the Ptp/Slitrk family (I), and general neuronal transcripts (J). Cells are color coded according to D1R+ and D2R+ identity. KS values are given for comparison of single-cell groups.

Data are means ± SEM. Asterisk indicates significant difference between groups (Mann-Whitney U test).

neurexin expression levels. Whole-tissue analysis compared prefrontal cortex (PFC), primary motor cortex (M1), ventral striatum (also known as the nucleus accumbens [NAc]), thalamus, and cerebellum to hippocampus across our entire synaptic cell-adhesion probe set (Figure S2). Then, we chose to further explore the NAc, as it displayed overall neurexin levels most similar to those in the hippocampus and comprises two major neuron subclasses whose mRNA expression profiles have been extensively characterized by fluorescence-activated cell sorting (FACS) analysis and BAC-trap methodologies (Heiman et al., 2008; Lobo, 2009). Specifically, the major principal neurons of the NAc are D1-receptor-positive (D1R+) medium spiny neurons (MSNs) that send their axons to the ventral tegmental area and D2-receptor-positive (D2R+) MSNs that project to the ventral pallidum (Grueter et al., 2012).

To investigate the neurexin profile of individual MSNs, we extracted cells from D1-Tomato BAC transgenic mice, which express tdTomato exclusively in D1R+ MSNs (Figure 3A) (Shuen et al., 2008). Fluorescently labeled cells were positive for D1R transcripts, while non-labeled cells strongly expressed D2R mRNAs (Figure 3B). Our single-cell data confirmed previous tissue-based expression analyses and assured us that visually guided pipette aspiration affords the precision to isolate single cells from a densely packed matrix of intermingling D1R+ and D2R+ MSNs (Figure 3B). Comparison of averaged single-cell neurexin expression levels between NAc D1R+ and D2R+ MSNs revealed significant cell-type-specific differences for Nrxn1α and Nrxn3β (Figures 3C and 3D). In contrast to the large splice-site diversity of hippocampal interneuron cell types, MSN cell types were similar, with the exception of Nrxn1 splice site 4 (ss4) probes. Furthermore, expression of neurexin ligands and Ptpr and Slitrk molecules was similar between MSN cell types (Figures 3E and 3F), precluding accurate clustering by all transcriptional profiles except neurexins (Figures

3G–3J). Taken together, these data indicate that cell-type-specific components of two distinct neural circuits display unique neurexin transcriptional repertoires.

Distinct Neurexin Splicing in Neurons Projecting to the Same Target

An alternative definition of cell type within neuronal circuits is the axonal target region (Kepecs and Fishell, 2014). Long-range projection neurons often have to navigate complex trajectories to reach specific areas where they eventually form synapses, and it is likely that they use extensive molecular instructions to achieve this (Zipursky and Sanes, 2010). To see whether specific patterns of neurexin expression could be supporting long-range target specificity, we identified individual projection neurons with a defined target destination by retrograde viral labeling techniques. First, we addressed convergent projections that target a common post-synaptic area by using RV-mediated retrograde tracing of NAc inputs from the PFC and midline thalamic nuclei, two major projection inputs to the NAc (Groenewegen and Berendse, 1994; Groenewegen et al., 1997). Retrograde uptake of a mutated RV, in which the rabies glycoprotein was replaced by an enhanced yellow fluorescent protein (EYFP) cassette (RV(ΔG)-EYFP), labeled PFC and thalamic neurons with restricted vGlut1 and Slitrk6 expression, respectively (Figures 4A and 4B). Single-cell profiling demonstrated that, despite their common synaptic target area, Nrxn3 transcriptional regulation was unique to each projection population (Figure 4D). While overall levels of Nrxn1α were similar in both populations, splice site 2 (ss2) and ss4 inclusion appeared to be regulated in a projection-specific manner (Figure 4C). Overall, strong clustering of both populations was observed for multiple probe sets (Figures 4G–4J). These data suggest that neurexin transcriptional profiles are not similar for neuronal populations with common projection targets.

To extend these findings and explore their generalizability, we profiled a functionally distinct neural circuit with an overall architecture similar to that of the NAc. We chose the dorsolateral striatum (DLS), as it is similarly composed of dopamine receptor-expressing MSNs that receive long-distance excitatory input from cortical regions and thalamic nuclei. Retrograde labeling via an RV expressing tdTomato (RV(ΔG)-tdTom) strongly labeled motor cortex and midline thalamus (Figure 5D). Isolated single neurons exhibited strikingly similar patterns of expression for regional markers that previously differentiated thalamic and cortical cells projecting to the NAc (compare Figures S3B and S3F). To simplify our comparison across experiments, we distilled neurexin expression profiles to the major transcriptional isoforms of Nrxn1 and Nrxn3, as well as splice site 3 (ss3), which previously demonstrated quantitative input-specific differences. While the overall transcriptional regulation of neurexins demonstrated similar input-specific patterns (compare Figures 5B and 5C with Figures 5E and 5F), differences were observed in ss3 regulation, particularly for Nrxn1 (Figures 5B and 5E, right panels). Taken together with the NAc data, it seems that cortical and thalamic domains have mRNA profiles that supersede specific circuit connectivity and that Nrxn1 and Nrxn3 transcriptional variants are part of this identity. However, specific splice isoforms of neurexins can be imposed on top of this regional code to create circuit-specific adhesion diversity.

Another possibility is that cortical and thalamic afferents display substantial bias in their connectivity within the striatum and that differences in neurexin profiles simply reflect cell-type-specific projections. To directly address this possibility, we used a pseudotyped-RV system previously used to transynaptically trace inputs to genetically defined cell types (Wickersham et al., 2007; Wall et al., 2013). Stereotaxic injection into D1R-Cre mice of an adeno-associated virus (AAV) expressing a Cre-recombinase-sensitive TVA receptor allowed for D1R+ MSN-specific uptake of EnvA-pseudotyped RV and subsequent retrograde synaptic transport (Figure 5G). Both medial PFC (mPFC) and midline thalamus were synaptically connected to NAc D1R+ MSNs (data not shown), and these neurons exhibited similar marker profiles to their region-specific counterparts (compare Figures S3B and S3J). Despite restricting our analysis to a single postsynaptic cell type, we continued to observe a highly divergent pattern of neurexin transcriptional regulation (compare Figures 5B and 5C with Figures 5H and 5I), strongly implying that postsynaptic targeting is not encoded by neurexin adhesion molecules.

To complement the aforementioned analysis, we explored divergent projections from a common origin. Specifically, we chose to examine neighboring PFC neurons with distinct synaptic target regions by simultaneously injecting the NAc with RV(ΔG)-EYFP and the lateral hypothalamus (l. Hyp) with RV(ΔG)-tdTOM (Figure 6A). Double RV injections labeled two adjacent populations of PFC cells with no discernable overlap (Figure 6A). In this set of experiments, neurexin transcriptional repertoires were identical between these two populations of divergently projecting neurons, although other transcriptional differences were readily observed (compare Figures 6C and 6D with Figures 6B and 6E; also, compare Figures 6G and 6I with Figure 6H). Taken together, the aforementioned approaches suggest that neurexin transcriptional profiles show characteristic, reproducible cell-type-specific differences across multiple brain regions and are not coordinated across connected circuit constituents (Figures S4B–S4E). Predictive sorting analysis (see Supplemental Experimental Procedures) further supported this conclusion, as neurexin transcriptional profiles were of high predictive value in distinguishing hippocampal interneurons and ventral striatal cell types (Figure S4F). They predicted these cell types much more effectively than other synaptic adhesion molecules or general neuronal transcripts, although somewhat less effectively than markers previously identified to have cell-type bias.

Single-Cell Regulation of the Neurexin Family

Numerous molecules are hypothesized to function cell autonomously to shape the splicing patterns of neurexins (Resnick et al., 2008; Rozic et al., 2011, 2013; Iijima et al., 2011, 2014). It is currently unclear, however, whether such splicing machinery directs individual neurons toward exclusive expression of single splice isoforms. To address this question, we analyzed the status of ss4 within Nrxn1 transcripts across multiple brain regions, as this locus has a single splice-site insertion (Figure 7A). Notably, we found that individual neurons were, indeed, capable of expressing both ss-IN and ss-OUT versions of ss4, although this configuration was highly dependent on the region analyzed

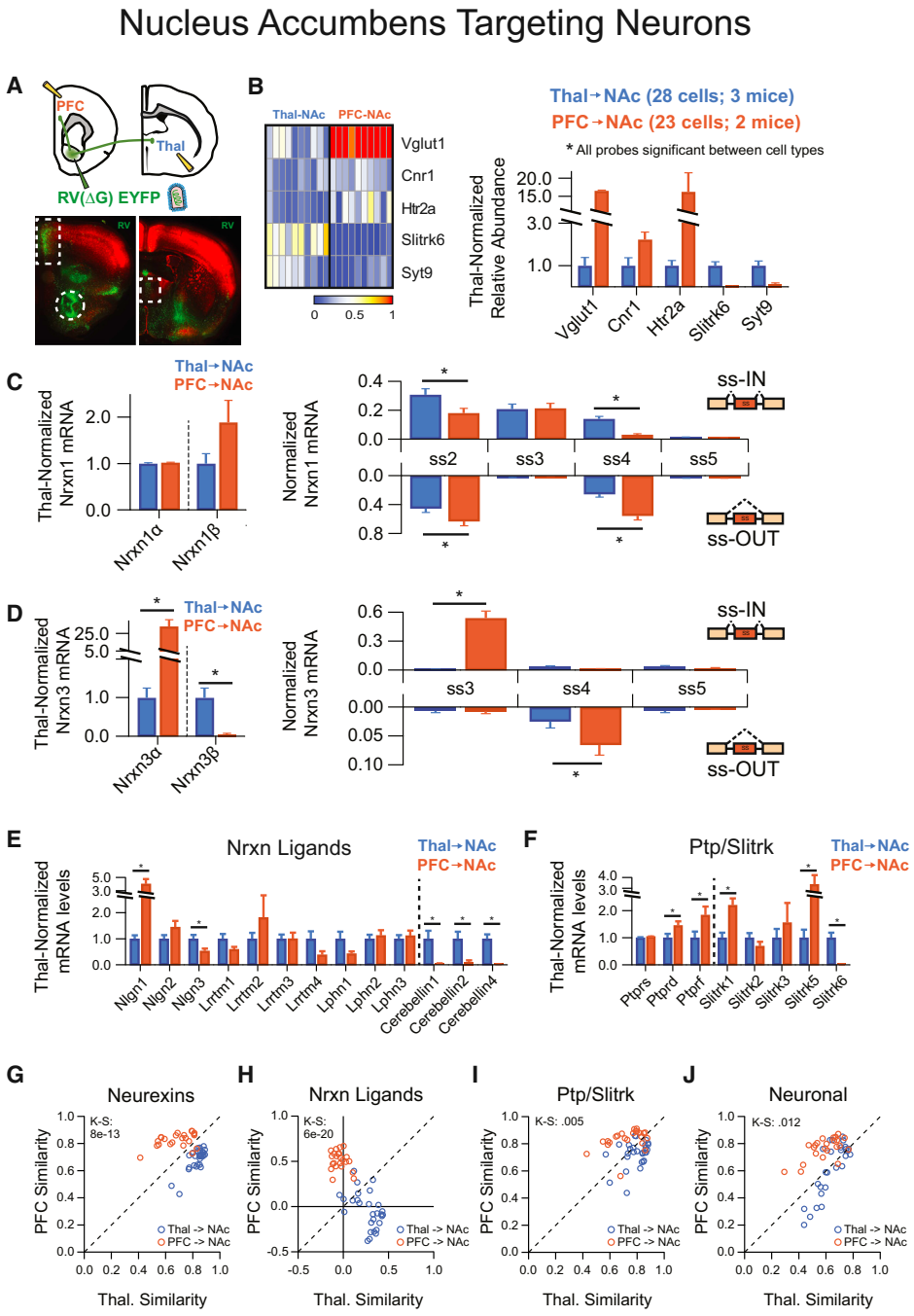

Figure 4. Two NAc-Targeting Neuronal Populations Do Not Share Neurexin Expression Patterns

(A) Top: strategy for single-cell isolation of NAc inputs by injection of RV(ΔG)-EYFP into the NAc core. Bottom: retrograde synaptic uptake of RV by neurons in the PFC (boxed, left picture) and midline thalamic nuclei (boxed, right picture) following injection into the NAc core (circle, left picture). Thal, thalamus.

(B) Left: heatmap representation of normalized expression of Thal → NAc and PFC → NAc for genes known to mark these subtypes. Right: averaged single-cell expression for Thal → NAc (n = 28) and PFC → NAc (n = 23), normalized to Thal → NAc values.

(C and D) Left: Nrxn α/β isoform expression, normalized to the average level in Thal → NAc cells. Right: splice-site graph showing averaged single-cell splice isoform expression values for ss-IN (upward bars) and ss-OUT (downward bars).

(E and F) Averaged single-cell normalized expression values for neurexin ligands (E) and the Ptp/Slitrk family (F).

(G–J) Pearson coefficient correlation plots demonstrating the similarity of individual neurons to the two cell classes being compared for neurexins (G), neurexin ligands (H), the Ptp/Slitrk family (I), and general neuronal transcripts (J). Cells are color coded according to Thal → NAc and Thal → NAc identity. KS values are given for comparison of single-cell groups.

Data are means ± SEM. Asterisk indicates significant difference between groups (Mann-Whitney U test).

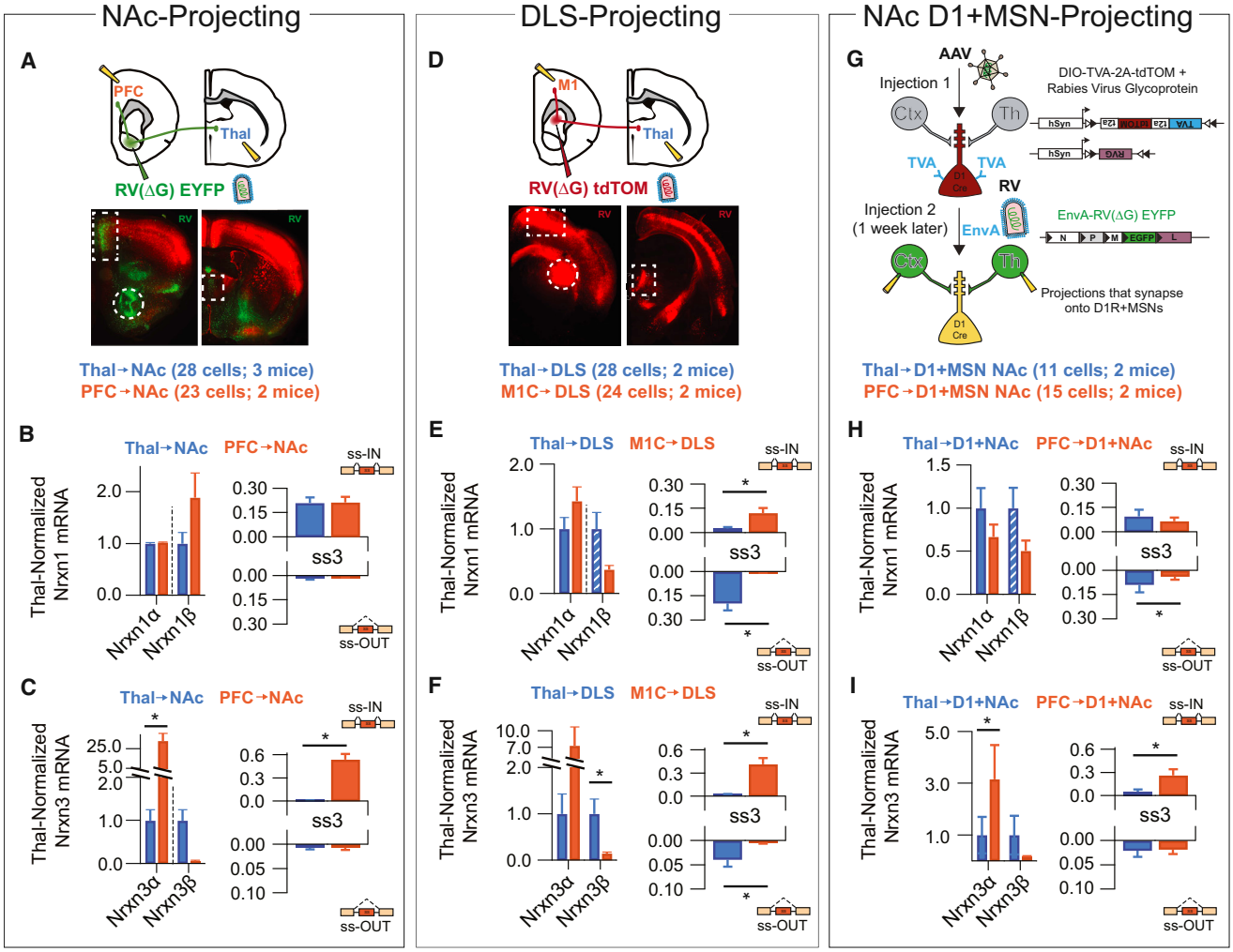

Figure 5. Comparison of Neurexin Expression Profiles across Diverse Striatal Circuits

(A–C) Data for NAc RV injection have been reproduced from Figure 4 for comparison purposes. Thal, thalamus.

(D) Top: strategy for single-cell isolation of DLS inputs by injection of RV(ΔG)-tdTOM into the DLS. Bottom: retrograde synaptic uptake of RV by neurons in M1 (boxed, left picture) and midline thalamic nuclei (boxed, right picture) following injection into DLS (circle, left picture).

(E and F) Thalamus-normalized expression of Nrxn1α/β (E, left) and Nrxn3α/β (F, left) in thalamo- (n = 28) and cortico (n = 24)-striatal projection neurons and normalized expression of Nrx1α, ss3 (E, right) and Nrxn3 α, ss3 (F, right).

(G) Top: strategy for single-cell isolation of NAc D1R+ MSN synaptic inputs by sequential injection procedure.

(H and I) Thalamus-normalized expression of Nrxn1α/β (H, left) and Nrxn3α/β (I, left) in thalamo- (n = 11) and cortico (n = 15)-accumbal projection neurons and normalized expression of Nrx1α, ss3 (H, right) and Nrxn3 α, ss3 (I, right).

Data are means ± SEM. Asterisk indicates significant difference between groups (Mann-Whitney U test).

(Figures 7B–7E). Cortical projection neurons largely excluded ss4 inserts, regardless of their target region (Figures 7D and 7E), whereas thalamic neurons projecting to the NAc and D1R+ MSNs found within this structure exhibited either ss4-IN, ss4-OUT, or coexpression of both species (Figures 7C and 7D). We also performed an alternative analysis to determine whether there was splice-site correlation across neurexin isoforms (i.e., between Nrxn1 and Nrxn3; Figure S5A). Again, we found that cortical projection neurons were nearly uniform in their transcriptional repertoire, with a robust exclusion of ss4 in both Nrxn1 and Nrxn3 (Figures S5D and S5E), while both CCK+ interneurons and thalamic projection neurons displayed coordinated ss4 exclusion as well as Nrxn1ss4-OUT/Nrxn3ss4-IN combinations (Figures S5B, S5D, and S5E).

Neurexin Transcriptional Signatures Are Altered in Response to Drug Exposure

Thus far, neurexin transcriptional profiles have been viewed as static characteristics with cell-type- and circuit-specific expression. Previous work suggests that activity-dependent processes can both alter the transcriptional diversity of neurexins (Rozic-Kotliroff and Zisapel, 2007; Resnick et al., 2008; Iijima et al., 2011; Rozic et al., 2011, 2013) and shape their function at developing synapses (Chubykin et al., 2007). To explore the potential

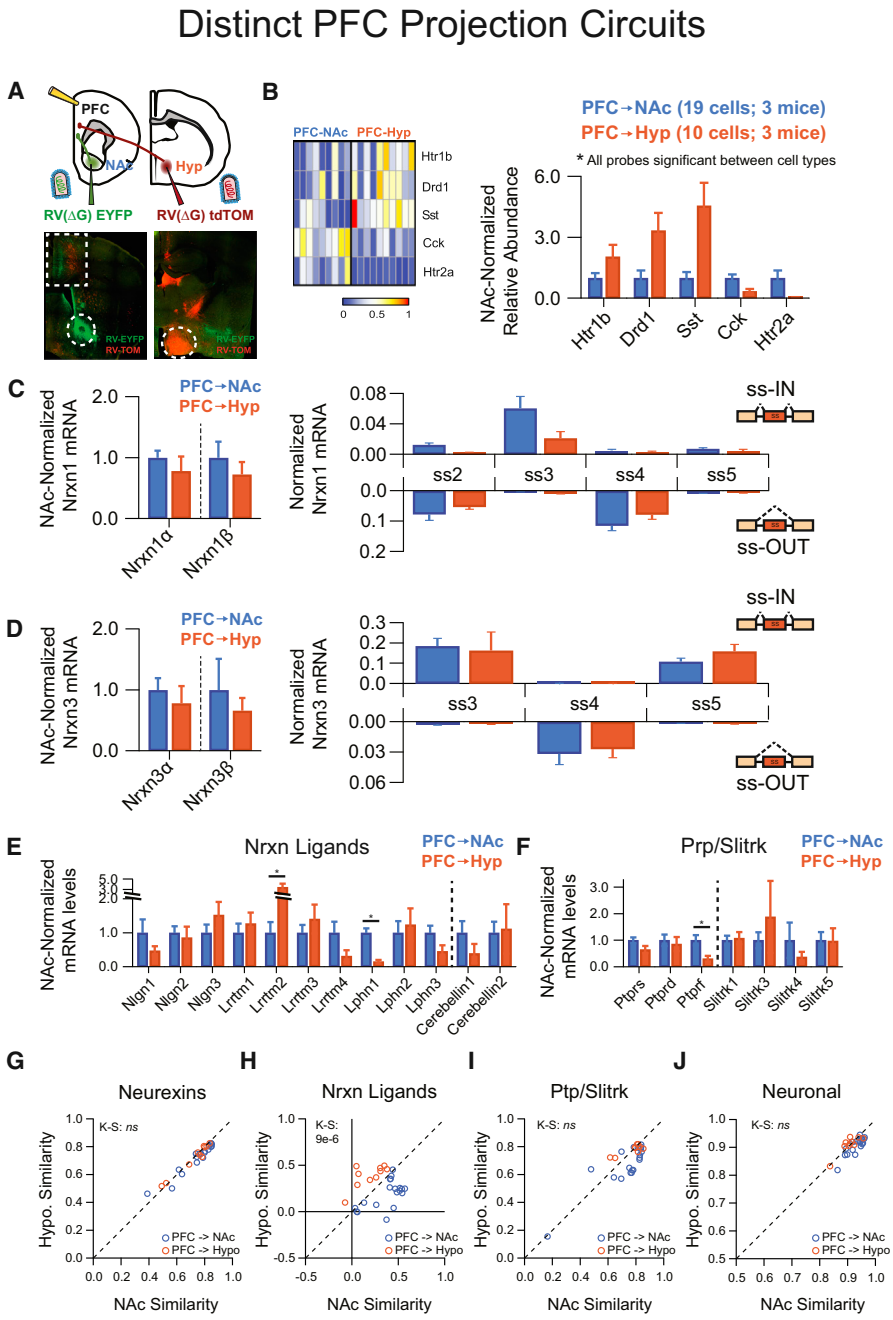

Figure 6. Neurexins Do Not Display Target-Region Specificity in Two Prefrontal Circuits

(A) Top: strategy for single-cell isolation of PFC neurons that project to NAc and hypothalamus (Hyp) by coinjection of RV(ΔG)-EYFP into the NAc core and RV(ΔG)-tdTOM into the hypothalamus. Bottom: retrograde synaptic uptake of RVs injected into NAc (left, circle) and hypothalamus (right, circle) by neurons in adjacent portions of the PFC (left, boxed region).

(B) Left: heatmap representation of normalized expression of PFC → NAc and PFC → Hyp for genes significantly different between these populations. Right: averaged single-cell expression for PFC → NAc (n = 19) and PFC → Hyp (n = 10), normalized to PFC → NAc values for each probe.

(C and D) Left: Nrxn α/β isoform expression, normalized by probe to the average level in PFC → NAc cells. Right: splice-site graph showing averaged single-cell splice isoform expression values for ss-IN (upward bars) and ss-OUT (downward bars).

(E and F) Averaged single-cell expression values for neurexin ligands (E) and the Ptp/Slitrk family (F), normalized to PFC → NAc values for each probe.

(G–J) Pearson coefficient correlation plots demonstrating the similarity of individual neurons to the two cell classes being compared for neurexins (G), neurexin ligands (H), the Ptp/Slitrk family (I), and general neuronal transcripts (J). Cells are color coded according to PFC → NAc and PFC → Hyp identity. KS values are given for comparison of single-cell groups.

Data are means ± SEM. Asterisk indicates significant difference between groups (Mann-Whitney U test).

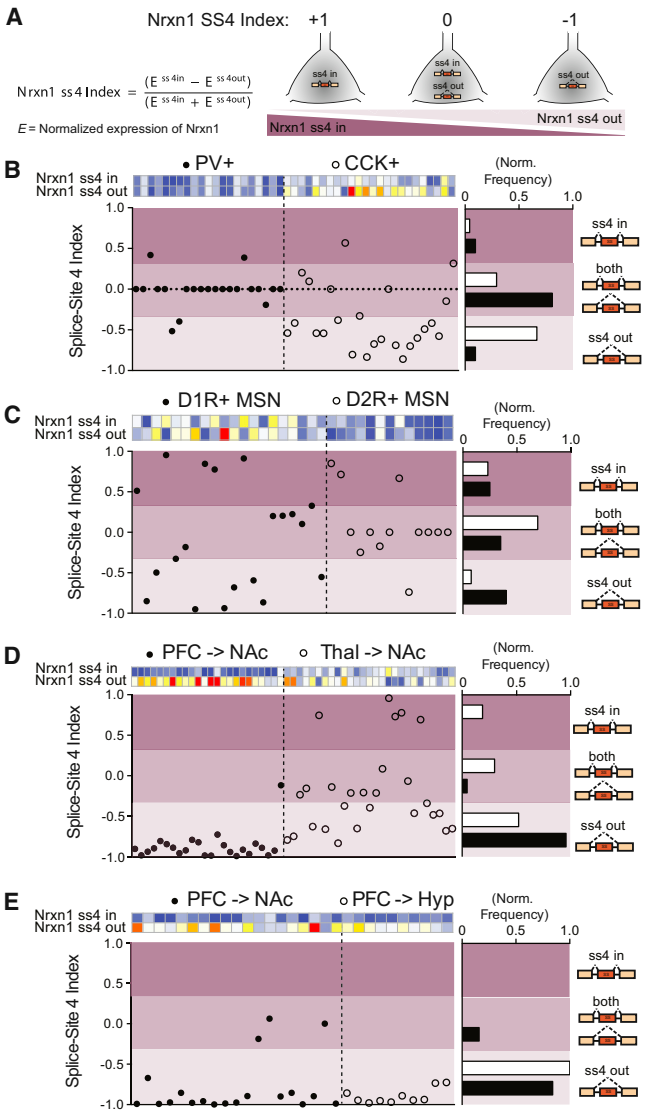

Figure 7. Single-Cell Regulation of Nrxn1 ss4 Selection Is Dependent on Brain Region

(A) Description of Nrxn1 ss4 index, which assesses the exclusive presence of single-splice isoforms or coexpression of Nrxn1 ss4-IN and Nrxn1 ss4-OUT transcripts. An index = 0 represents roughly equal normalized expression values for both Nrx1 ss4-IN and Nrxn1 ss4-OUT probes.

(B–E) Plot of ss4 index for all single neurons collected in hippocampal interneuron (B, n = 45 cells), NAc MSN (C, n = 33 cells), NAc-projecting (D, n = 51 cells), and divergent PFC projection (E, n = 29 cells) experiments. Each plot shows the heatmaps of both Nrx1 ss4 probes for each cell, with the ss4 index plotted below. Splice-site territories were arbitrarily subdivided into ss4-IN (index = 0.33–1.00), ss4-IN and ss4-OUT (index = −0.33–0.33), and ss4-OUT (index = −1.0 to −0.33), and normalized (Norm.) frequencies were calculated for each region (right histograms). Thal, midline thalamic nuclei; Hyp, hypothalamus.

for plasticity of neurexin transcriptional repertoires, we exposed animals to chronic non-contingent cocaine administration, an experience known to cause major synaptic alterations within NAc circuitry (Bowers et al., 2010; Grueter et al., 2012). Mice exposed to 5 consecutive days of cocaine developed robust behavioral sensitization, which was manifest by a dramatic increase in locomotor activity, as compared to saline-injected controls (Figures 8A and 8B). D1R+ MSNs extracted 3 hr after the last cocaine treatment displayed modest transcriptional changes, including an increase in the Gria4 subunit of AMPA receptors (AMPARs) and a decrease in Lrrtm4 (Figures 8C and 8F). Despite this, no change in the neurexin transcription or splice code was observed (Figures 8D and 8E) in these cells. In contrast, D2R+ MSNs from cocaine-injected mice displayed both modest changes in AMPAR transcripts, as well as large (>50%) reductions in total Nrxn1 transcriptional activity (Figures 8G and 8H). In addition, these changes were accompanied by differential expression of specific isoforms of both Nrxn1 and Nrxn3 (Figures 8H and 8I). Together, these data uncover a cell-type-specific remodeling of neurexin codes at the single-cell level following chronic exposure to a drug of abuse.

DISCUSSION

Understanding the molecular machinery that defines circuit and synapse specificity is a daunting challenge with enormous clinical and therapeutic implications. Synaptic adhesion molecules in general, and neurexins in particular, have been proposed to contribute to circuit formation within the nervous system (Aoto et al., 2013; Futai et al., 2013; Ullrich et al., 1995; Ushkaryov et al., 1992). Here, we used single-cell qRT-PCR to illuminate the expression profiles and differential splicing of neurexin mRNAs from individual neurons embedded in mature neural circuits. These experiments are the first to address at the single-neuron level the existence of a "synaptic adhesion code"—a regulated, combinatorial expression of synaptic adhesion molecules that could contain molecular instructions for the hierarchical organization of synapses, including the connectivity of specific neuronal populations, the precise sub-cellular localization of synaptic contacts, the specific strength and molecular composition of these connections, and their ability to be modified by the environment (see Figure S6). By combining genetic and viral circuit mapping techniques, microfluidics technology, and a novel qPCR probe design, we assessed the contributions of neurexin transcriptional diversity to such codes. First, we found that single-neuron analysis of hippocampal CA1 transcriptional profiles had several advantages over tissue mRNA sampling, including lower detection levels of genes commonly associated with glial populations, unparalleled access to sparse neuronal populations, and invaluable estimates of the variance of transcript expression within neuronal populations. Second, by using this technique, we reached several conclusions regarding neurexins that could not have been demonstrated otherwise. (1) Neurexins exhibit cell-type-specific expression patterns that are reproducible across neurons; (2) neurons with common long-range projection targets or cell-type-specific connectivity do not necessarily use similar neurexin transcriptional codes; (3) coordination of neurexin alternative splicing is specific to brain regions; and (4) neurexin expression profiles can be altered in a cell-type-specific manner in response to chronic cocaine treatment.

Recent deep-sequencing technologies have provided in-depth and comprehensive cataloging of potential neurexin

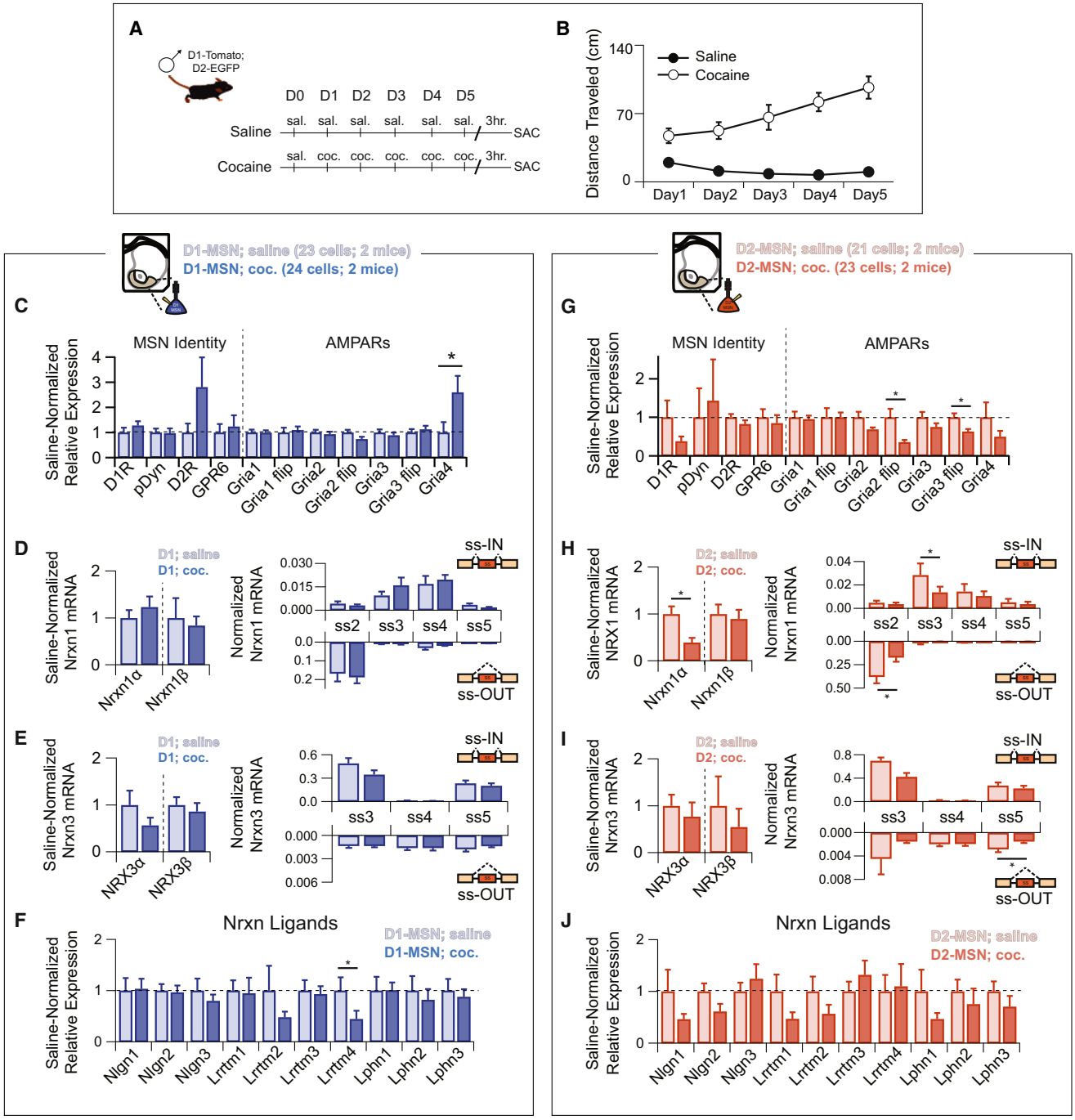

Figure 8. Neurexin Transcriptional Profiles Undergo Cell-Type-Specific Changes during the Development of Cocaine-Evoked Behavioral Sensitization

(A) Behavioral paradigm for 5-day non-contingent cocaine administration. D1-Tom/D2-EGFP transgenic mice were sacrificed (SAC) 3 hr after final cocaine injection. (B) Behavioral sensitization was manifest by steady increase in locomotor activity in the cocaine group as compared with saline controls over sequential days of cocaine administration.

(C–J) In (C and G), averaged single-cell expression is shown for markers of MSN identity and AMPA subtype glutamate receptors for saline- versus cocaine-treated mice of D1R+ (C) and D2R+ (G) MSN subtype, with expression values normalized to the saline controls for each probe. (D and H) Left: Averaged single-cell expression of Nrxn1 isoforms for saline- versus cocaine-treated mice of D1R+ (D) and D2R+ (H) MSN subtype, with expression values normalized to the saline controls for each probe. Right: Splice-site graph showing averaged single-cell splice isoform expression values for ss-IN (upward bars) and ss-OUT (downward bars) for saline- versus cocaine-treated mice of D1R+ (D) and D2R+ (H) MSN subtype. (E and I) Left: Averaged single-cell expression of Nrxn3 isoforms for saline- versus cocaine-treated mice of D1R+ (E) and D2R+ (I) MSN subtype, with expression values normalized to saline controls for each probe. Right: Splice-site graph

(legend continued on next page)

transcriptional repertoires from whole-brain, PFC, and cerebellar granule cell cultures (Treutlein et al., 2014; Schreiner et al., 2014). While these molecule-centered sequencing approaches nearly mapped the full extent of neurexin diversity, technical limitations required large sample input, making it impossible to assess whether individual neurons regulate neurexin diversity to encode synaptic connectivity within neural circuits. Our data directly address this problem by demonstrating reproducible cell-type- and circuit-specific expression of different families of Nrxns as well as other synaptic adhesion molecules. Exploration of the neurexin transcriptional repertoire of hippocampal GABAergic interneurons and striatal MSNs suggested that neurexin expression is tightly and reproducibly regulated at the single-cell level. How this transcriptional diversity is achieved depends on the brain region: MSNs may exclusively utilize promoter selection to control transcriptional output, while basket cell populations additionally use post-transcriptional splicing to enhance differences in their neurexin profiles. Further work will be needed to determine whether the enhanced neurexin transcriptional divergence of interneurons, as compared to MSNs, is related to the unique developmental origins of the PV+ and CCK+ cells, their different activity levels, or their particular splicing machinery (Rozic-Kotliroff and Zisapel, 2007; Resnick et al., 2008; Tricoire et al., 2011; Ehrmann et al., 2013; Iijima et al., 2014; See et al., 2014), as well as whether these differences have a functional role in specifying the distinct synaptic properties of these diverse subclasses.

A series of experiments performed to probe the correlation between synaptic target area and neurexin expression profile suggest that neurexins alone do not encode target specificity. Cortical and thalamic afferent projection neurons were examined for functionally and anatomically distinct striatal circuits and revealed highly divergent input-specific neurexin profiles. However, although individual cortical or thalamic populations of neurons participate in non-overlapping cortico-striato-thalamic circuits, comparisons between these populations of neurons demonstrated conserved regulation of neurexin transcription, with differences restricted to splice-site utilization. These results raise the intriguing possibility that splice-site control provides an alternative evolutionary mechanism for diversification of neurexin expression patterns from regionally conserved templates. Further analysis of a cortico-striato-thalamic circuit synaptically connected to D1R+ MSNs demonstrated that input-specific neurexin profiles are also not a result of biased-cell-type connectivity. In contrast to these data, PFC neurons projecting to the hypothalamus and NAc inhabited distinct cortical layers but still exhibited identical neurexin expression patterns. Together, these data make a strong argument that target region is not encoded by neurexin diversity, consistent with previous reports that α-neurexin knockout mice do not display deficits in axonal projections of olfactory circuits (Dudanova et al., 2007). Furthermore, we demonstrate that neurexin profiles do not encode cell-type-specific connectivity, suggesting that it is unlikely that neurexins function as a map on which patterns of neuronal connectivity are established.

Our analyses exploring single-cell relationships between individual neurexin splice isoforms could have substantial implications for understanding the genetics of neuropsychiatric illness, as this gene family is extensively linked to human neuropsychiatric disease (Elia et al., 2010; Pinto et al., 2010; Tam et al., 2009). Understanding how mutations in neurexins eventually lead to behavioral abnormalities requires the discovery of "molecularly vulnerable circuits," specific neuronal populations that cannot functionally compensate for gene mutations because they lack genetic redundancy or are inherently vulnerable to small changes in synapse properties (Rothwell et al., 2014; Soler-Llavina et al., 2011). Coordinated cellular splicing of Nrxns could be an important source of such molecular redundancy, as evidenced by the interchangeability of neurexin isoforms lacking ss4 for the maintenance of AMPAR function (Aoto et al., 2013). Following this logic, cortical projection neurons—which exclusively coordinate, via alternative splicing, Nrxn1 and Nrxn3 ss4 exclusion—are unlikely to be as vulnerable to single-gene loss as NAc-projecting thalamic neurons, which could not use Nrxn3 expression to replace Nrxn1 deficiencies because of conflicting splice-site usage. Unfortunately, transcriptional patterns read out at the soma provide little information about the targeting of mRNA populations to specific dendritic or axonal compartments. If synaptic adhesion molecules are recruited in a synapse-specific manner, mutations may uniquely perturb select sets of inputs. Nonetheless, single-neuron transcriptional analyses of this sort clearly provide a powerful new tool for the prediction of molecularly vulnerable disease-relevant circuits in the future.

If neurexins do encode cell-type-specific information about synaptic function, understanding their potential for plasticity could provide essential mechanistic information about how neural circuits modify themselves in response to environmental experience. To explore this, we chronically administered cocaine to mice and detailed how their synaptic adhesion profiles changed during behavioral sensitization. Surprisingly, 5 days of cocaine administration demonstrated remarkably subtle effects on the overall transcriptional profiles of NAc MSNs, which are known to undergo significant synaptic remodeling 2 weeks following cocaine exposure (Huang et al., 2009; Kim et al., 2011; Russo et al., 2010). However, we observed an ~50% downregulation of Nrxn1α transcripts exclusively in D2R+ MSNs, along with decreases in the abundance of ss2-OUT and ss3-IN isoforms. Previous work has demonstrated activity-dependent changes in neurexin alternative splicing (Patzke and Ernsberger, 2000; Rozic-Kotliroff and Zisapel, 2007; Rozic et al., 2013; Iijima et al., 2014). Previous reports, together with our data, make it clear that the pattern of neurexin splicing in the nervous system is sensitive to a range of physiological stimuli. While more work is required to understand the significance of both baseline adhesion profiles and behaviorally induced

showing averaged single-cell splice isoform expression values for ss-IN (upward bars) and ss-OUT (downward bars) for saline- versus cocaine-treated mice of D1R+ (E) and D2R+ (I) MSN subtype. (F and J) Averaged single-cell expression of neurexin ligands for saline- versus cocaine-treated mice of D1R+ (F) and D2R+ (J) subtype, with expression values normalized to the saline controls for each probe.

Data are means ± SEM. Asterisk indicates significant difference between groups (Mann-Whitney U test).

alterations, we believe that our single-cell analysis of synaptic adhesion molecule transcription provides a broad foundation for understanding how molecules encode synaptic function and how this is altered by the environment and disease.

EXPERIMENTAL PROCEDURES

Animals

All procedures conformed to the NIH Guidelines for the Care and Use of Laboratory Animals and were approved by the Stanford University Administrative Panel on Laboratory Animal Care.

Single-Cell Transcriptional Profiling

Acute brain slices were cut, and patch pipettes were used for cytosol extraction. Samples then underwent reverse transcription and target-specific amplification, followed by qPCR. Further details are found in Supplemental Experimental Procedures.

Primetime Assay Design

All Primetime assays were ordered from Integrated DNA Technologies (IDT). Assays were designed to generate amplicons of 70–100 bp in length that bridged exon-intron junctions. Wherever possible, ss-IN- and ss-OUT-specific assays differed by only a single primer. The complexity of neurexin splicing is such that ss-IN can include many similar exons differentiated by only a few amino acids. In these instances, effort was taken to design primers that would recognize the largest number of potential ss-IN products. Probes passing efficiency criteria (>90%) as described by

$$Amplication\ Efficiency = 10^{(-1/slope)} - 1$$

were subjected to qPCR with plasmid templates of known neurexin splicing combinations to test for probe specificity. The final probe set included 170 probes, 146 of which were unique (see Table S1 for sequences).

Data Analysis

All Ct data were calculated by Biomark acquisition software, exported as .csv files, and analyzed in Mathematica version 9.0 (Wolfram Research) with custom written protocols. Each chip run included eight tissue cDNA dilutions to monitor the efficiencies of probes across experiments. Ct values were converted to normalized expression levels by the following formula:

$$Norm.\ Expression^{ProbeA} = 2^{Ct^{probeA} - Ct^{norm.\ probes}},$$

where $Ct^{norm.\ probes}$ is the average Ct of two Actb probes and Atp1b1. With these normalizer probes, nearly all expression values fell between 0 and 1. Single cells, whose normalizer value was ±2 cycles from overall normalizer average, were omitted from further analysis. In nucleus accumbens experiments, Lhx8+ cells were removed from the dataset, as they likely represented cholinergic interneurons (Zhao et al., 2003); all other cells were analyzed. Heatmaps were generated with the ArrayPlot function in Mathematica and scaled to the highest and lowest global normalized expression values in a given dataset. For data sorting, cell type was always defined by transgenic mouse line or viral labeling. Expression values were compared between two defined cell populations using Mann-Whitney U test, with significance set at $p < 0.05$. Tissue versus single-cell comparisons were analyzed using two-way ANOVA followed by Tukey's multiple comparison post hoc tests. All summary expression data are displayed as mean ± SEM. With the exception of splice-site-specific probes, expression was normalized to the first cell type in each respective figure (B–F in Figures 2, 3, 4, and 6). All comparisons were made between cell types for each probe to avoid confounding cross-probe differences in sensitivity.

Clustering

Clustering was used to group cells by similarity of transcriptional profile. For each chip, probes were rank-ordered by overall population variance, and the top 50% of high-variance probes were used for clustering. Probe groups included: Neurexins (Nrxn1α, Nrxn1β, Nrxn3α, Nrx3β, and all Nrxn1 and Nrxn3 splice sites); neurexin ligands (Nlgn1–3, Lrrtm1–4, Lphn1–3, Crbln1, Crbln2, and Crbln4); Ptp/Slitrk (Ptprs, Ptprd, Ptprf, and Slitrk1–6); and neuronal (NeuN, Nefl, Mapt, Gad65, Syt1, Vamp3, Grm1, and Grm5). Pearson's correlation coefficient ("Correlation" function in Mathematica) was calculated between all cells, and single-cell matrices were created describing the correlation of each cell to the two experimental populations. Cluster plots were assayed for significance using the Kolmogarov-Smirnov test.

Predictive Sorting

Predictive sorting was used to test the efficacy of transcriptional profiles in distinguishing cell-type identity. In brief, single-cell data were analyzed by the "ClusteringComponents" function in Mathematica (Euclidean distance function for 500 sequential iterations) to create two cell populations (group A and group B). The following formula was used to create a weighted predictive sorting measure:

$$Accuracy = \left(\frac{N_A^{correct}}{N_A^{total}}\right)\left(\frac{N_A^{total}}{N}\right) + \left(\frac{N_B^{correct}}{N_B^{total}}\right)\left(\frac{N_B^{total}}{N}\right),$$

where N = the total number of single cells, N_A = cells in group A, and N_B = cells in group B.

SUPPLEMENTAL INFORMATION

Supplemental Information includes Supplemental Experimental Procedures, six figures, and one table and can be found with this article online at http://dx.doi.org/10.1016/j.neuron.2015.06.028.

AUTHOR CONTRIBUTIONS

M.V.F., C.F., O.G., R.C.M., and T.C.S. designed the study. M.V.F. and C.F. analyzed Fluidigm datasets. M.V.F., C.F., and P.E.R. picked cells for transcriptional analysis. O.G. isolated tissue mRNA. O.G. designed all Neurexin-specific assays, and C.F. designed AMPAR-specific probe sets. M.V.F. and O.G. determined assay efficiencies and specificities. P.E.R. performed behavioral sensitization experiments. G.L.S. performed rabies virus injections, tissue histology, and image acquisition. M.V.F., C.F., R.C.M., and T.C.S. wrote and edited the manuscript.

ACKNOWLEDGMENTS

We thank Atiyeh Afjei for technical assistance, as well as Ami Citri and all members of the R.C.M./T.C.S. laboratories for helpful discussions. We also thank Byungkook Lim and Kevin Beier for their kind gifts of rabies virus aliquots. This work was supported by grants from the National Institute of Mental Health (P50 MH086403 to R.C.M., R37MH52804 to T.C.S., and K99 MH099243 to M.V.F.) and National Institute on Drug Abuse (K99DA034029 to C.F., P01 DA008227 to R.C.M., K99DA038112 to O.G., and K99DA037279 to P.E.R.).

Received: January 4, 2015
Revised: June 10, 2015
Accepted: June 17, 2015
Published: July 15, 2015

REFERENCES

Aoto, J., Martinelli, D.C., Malenka, R.C., Tabuchi, K., and Südhof, T.C. (2013). Presynaptic neurexin-3 alternative splicing trans-synaptically controls postsynaptic AMPA receptor trafficking. Cell *154*, 75–88.

Araç, D., Boucard, A.A., Ozkan, E., Strop, P., Newell, E., Südhof, T.C., and Brunger, A.T. (2007). Structures of neuroligin-1 and the neuroligin-1/neurexin-1 beta complex reveal specific protein-protein and protein-Ca2+ interactions. Neuron *56*, 992–1003.

Boucard, A.A., Chubykin, A.A., Comoletti, D., Taylor, P., and Südhof, T.C. (2005). A splice code for trans-synaptic cell adhesion mediated by binding of neuroligin 1 to alpha- and beta-neurexins. Neuron *48*, 229–236.

Boucard, A.A., Maxeiner, S., and Südhof, T.C. (2014). Latrophilins function as heterophilic cell-adhesion molecules by binding to teneurins: regulation by alternative splicing. J. Biol. Chem. *289*, 387–402.

Bowers, M.S., Chen, B.T., and Bonci, A. (2010). AMPA receptor synaptic plasticity induced by psychostimulants: the past, present, and therapeutic future. Neuron *67*, 11–24.

Chen, S.X., Tari, P.K., She, K., and Haas, K. (2010). Neurexin-neuroligin cell adhesion complexes contribute to synaptotropic dendritogenesis via growth stabilization mechanisms in vivo. Neuron *67*, 967–983.

Chen, F., Venugopal, V., Murray, B., and Rudenko, G. (2011). The structure of neurexin 1α reveals features promoting a role as synaptic organizer. Structure *19*, 779–789.

Chubykin, A.A., Atasoy, D., Etherton, M.R., Brose, N., Kavalali, E.T., Gibson, J.R., and Südhof, T.C. (2007). Activity-dependent validation of excitatory versus inhibitory synapses by neuroligin-1 versus neuroligin-2. Neuron *54*, 919–931.

Comoletti, D., Miller, M.T., Jeffries, C.M., Wilson, J., Demeler, B., Taylor, P., Trewhella, J., and Nakagawa, T. (2010). The macromolecular architecture of extracellular domain of alphaNRXN1: domain organization, flexibility, and insights into trans-synaptic disposition. Structure *18*, 1044–1053.

de Wit, J., Sylwestrak, E., O'Sullivan, M.L., Otto, S., Tiglio, K., Savas, J.N., Yates, J.R., 3rd, Comoletti, D., Taylor, P., and Ghosh, A. (2009). LRRTM2 interacts with Neurexin1 and regulates excitatory synapse formation. Neuron *64*, 799–806.

Duan, X., Krishnaswamy, A., De la Huerta, I., and Sanes, J.R. (2014). Type II cadherins guide assembly of a direction-selective retinal circuit. Cell *158*, 793–807.

Dudanova, I., Tabuchi, K., Rohlmann, A., Südhof, T.C., and Missler, M. (2007). Deletion of alpha-neurexins does not cause a major impairment of axonal pathfinding or synapse formation. J. Comp. Neurol. *502*, 261–274.

Ehrmann, I., Dalgliesh, C., Liu, Y., Danilenko, M., Crosier, M., Overman, L., Arthur, H.M., Lindsay, S., Clowry, G.J., Venables, J.P., et al. (2013). The tissue-specific RNA binding protein T-STAR controls regional splicing patterns of neurexin pre-mRNAs in the brain. PLoS Genet. *9*, e1003474.

Elia, J., Gai, X., Xie, H.M., Perin, J.C., Geiger, E., Glessner, J.T., D'arcy, M., deBerardinis, R., Frackelton, E., Kim, C., et al. (2010). Rare structural variants found in attention-deficit hyperactivity disorder are preferentially associated with neurodevelopmental genes. Mol. Psychiatry *15*, 637–646.

Földy, C., Lee, S.Y., Szabadics, J., Neu, A., and Soltesz, I. (2007). Cell type-specific gating of perisomatic inhibition by cholecystokinin. Nat. Neurosci. *10*, 1128–1130.

Freund, T.F. (2003). Interneuron Diversity series: Rhythm and mood in perisomatic inhibition. Trends Neurosci. *26*, 489–495.

Freund, T.F., and Katona, I. (2007). Perisomatic inhibition. Neuron *56*, 33–42.

Futai, K., Doty, C.D., Baek, B., Ryu, J., and Sheng, M. (2013). Specific transsynaptic interaction with inhibitory interneuronal neurexin underlies differential ability of neuroligins to induce functional inhibitory synapses. J. Neurosci. *33*, 3612–3623.

Groenewegen, H.J., and Berendse, H.W. (1994). The specificity of the 'nonspecific' midline and intralaminar thalamic nuclei. Trends Neurosci. *17*, 52–57.

Groenewegen, H.J., Wright, C.I., and Uylings, H.B. (1997). The anatomical relationships of the prefrontal cortex with limbic structures and the basal ganglia. J. Psychopharmacol. (Oxford) *11*, 99–106.

Grueter, B.A., Rothwell, P.E., and Malenka, R.C. (2012). Integrating synaptic plasticity and striatal circuit function in addiction. Curr. Opin. Neurobiol. *22*, 545–551.

Heiman, M., Schaefer, A., Gong, S., Peterson, J.D., Day, M., Ramsey, K.E., Suárez-Fariñas, M., Schwarz, C., Stephan, D.A., Surmeier, D.J., et al. (2008). A translational profiling approach for the molecular characterization of CNS cell types. Cell *135*, 738–748.

Hippenmeyer, S., Huber, R.M., Ladle, D.R., Murphy, K., and Arber, S. (2007). ETS transcription factor Erm controls subsynaptic gene expression in skeletal muscles. Neuron *55*, 726–740.

Huang, Y.H., Lin, Y., Mu, P., Lee, B.R., Brown, T.E., Wayman, G., Marie, H., Liu, W., Yan, Z., Sorg, B.A., et al. (2009). In vivo cocaine experience generates silent synapses. Neuron *63*, 40–47.

Iijima, T., Wu, K., Witte, H., Hanno-Iijima, Y., Glatter, T., Richard, S., and Scheiffele, P. (2011). SAM68 regulates neuronal activity-dependent alternative splicing of neurexin-1. Cell *147*, 1601–1614.

Iijima, T., Iijima, Y., Witte, H., and Scheiffele, P. (2014). Neuronal cell type-specific alternative splicing is regulated by the KH domain protein SLM1. J. Cell Biol. *204*, 331–342.

Kepecs, A., and Fishell, G. (2014). Interneuron cell types are fit to function. Nature *505*, 318–326.

Kim, J., Park, B.H., Lee, J.H., Park, S.K., and Kim, J.H. (2011). Cell type-specific alterations in the nucleus accumbens by repeated exposures to cocaine. Biol. Psychiatry *69*, 1026–1034.

Klausberger, T., and Somogyi, P. (2008). Neuronal diversity and temporal dynamics: the unity of hippocampal circuit operations. Science *321*, 53–57.

Linhoff, M.W., Laurén, J., Cassidy, R.M., Dobie, F.A., Takahashi, H., Nygaard, H.B., Airaksinen, M.S., Strittmatter, S.M., and Craig, A.M. (2009). An unbiased expression screen for synaptogenic proteins identifies the LRRTM protein family as synaptic organizers. Neuron *61*, 734–749.

Lobo, M.K. (2009). Molecular profiling of striatonigral and striatopallidal medium spiny neurons past, present, and future. Int. Rev. Neurobiol. *89*, 1–35.

Madisen, L., Zwingman, T.A., Sunkin, S.M., Oh, S.W., Zariwala, H.A., Gu, H., Ng, L.L., Palmiter, R.D., Hawrylycz, M.J., Jones, A.R., et al. (2010). A robust and high-throughput Cre reporting and characterization system for the whole mouse brain. Nat. Neurosci. *13*, 133–140.

Missler, M., Zhang, W., Rohlmann, A., Kattenstroth, G., Hammer, R.E., Gottmann, K., and Südhof, T.C. (2003). Alpha-neurexins couple Ca2+ channels to synaptic vesicle exocytosis. Nature *423*, 939–948.

Patzke, H., and Ernsberger, U. (2000). Expression of neurexin Ialpha splice variants in sympathetic neurons: selective changes during differentiation and in response to neurotrophins. Mol. Cell. Neurosci. *15*, 561–572.

Pinto, D., Pagnamenta, A.T., Klei, L., Anney, R., Merico, D., Regan, R., Conroy, J., Magalhaes, T.R., Correia, C., Abrahams, B.S., et al. (2010). Functional impact of global rare copy number variation in autism spectrum disorders. Nature *466*, 368–372.

Resnick, M., Segall, A., Rozic-Kotliroff, G., Lupowitz, Z., and Zisapel, N. (2008). Alternative splicing of neurexins: a role for neuronal polypyrimidine tract binding protein. Neurosci. Lett. *439*, 235–240.

Rothwell, P.E., Fuccillo, M.V., Maxeiner, S., Hayton, S.J., Gokce, O., Lim, B.K., Fowler, S.C., Malenka, R.C., and Südhof, T.C. (2014). Autism-associated neuroligin-3 mutations commonly impair striatal circuits to boost repetitive behaviors. Cell *158*, 198–212.

Rozic, G., Lupowitz, Z., Piontkewitz, Y., and Zisapel, N. (2011). Dynamic changes in neurexins' alternative splicing: role of Rho-associated protein kinases and relevance to memory formation. PLoS ONE *6*, e18579.

Rozic, G., Lupowitz, Z., and Zisapel, N. (2013). Exonal elements and factors involved in the depolarization-induced alternative splicing of neurexin 2. J. Mol. Neurosci. *50*, 221–233.

Rozic-Kotliroff, G., and Zisapel, N. (2007). Ca2+ -dependent splicing of neurexin IIalpha. Biochem. Biophys. Res. Commun. *352*, 226–230.

Russo, S.J., Dietz, D.M., Dumitriu, D., Morrison, J.H., Malenka, R.C., and Nestler, E.J. (2010). The addicted synapse: mechanisms of synaptic and structural plasticity in nucleus accumbens. Trends Neurosci. *33*, 267–276.

Schreiner, D., Nguyen, T.-M., Russo, G., Heber, S., Patrignani, A., Ahrné, E., and Scheiffele, P. (2014). Targeted combinatorial alternative splicing generates brain region-specific repertoires of neurexins. Neuron *84*, 386–398.

See, K., Yadav, P., Giegerich, M., Cheong, P.S., Graf, M., Vyas, H., Lee, S.G., Mathavan, S., Fischer, U., Sendtner, M., and Winkler, C. (2014). SMN

deficiency alters Nrxn2 expression and splicing in zebrafish and mouse models of spinal muscular atrophy. Hum. Mol. Genet. *23*, 1754–1770.

Shuen, J.A., Chen, M., Gloss, B., and Calakos, N. (2008). Drd1a-tdTomato BAC transgenic mice for simultaneous visualization of medium spiny neurons in the direct and indirect pathways of the basal ganglia. J. Neurosci. *28*, 2681–2685.

Siddiqui, T.J., Pancaroglu, R., Kang, Y., Rooyakkers, A., and Craig, A.M. (2010). LRRTMs and neuroligins bind neurexins with a differential code to cooperate in glutamate synapse development. J. Neurosci. *30*, 7495–7506.

Soler-Llavina, G.J., Fuccillo, M.V., Ko, J., Südhof, T.C., and Malenka, R.C. (2011). The neurexin ligands, neuroligins and leucine-rich repeat transmembrane proteins, perform convergent and divergent synaptic functions in vivo. Proc. Natl. Acad. Sci. USA *108*, 16502–16509.

Soler-Llavina, G.J., Arstikaitis, P., Morishita, W., Ahmad, M., Südhof, T.C., and Malenka, R.C. (2013). Leucine-rich repeat transmembrane proteins are essential for maintenance of long-term potentiation. Neuron *79*, 439–446.

Südhof, T.C. (2008). Neuroligins and neurexins link synaptic function to cognitive disease. Nature *455*, 903–911.

Tabuchi, K., and Südhof, T.C. (2002). Structure and evolution of neurexin genes: insight into the mechanism of alternative splicing. Genomics *79*, 849–859.

Takahashi, H., and Craig, A.M. (2013). Protein tyrosine phosphatases PTPδ, PTPσ, and LAR: presynaptic hubs for synapse organization. Trends Neurosci. *36*, 522–534.

Tam, G.W., Redon, R., Carter, N.P., and Grant, S.G. (2009). The role of DNA copy number variation in schizophrenia. Biol. Psychiatry *66*, 1005–1012.

Treutlein, B., Gökce, O., Quake, S.R., and Südhof, T.C. (2014). Cartography of neurexin alternative splicing mapped by single-molecule long-read mRNA sequencing. Proc. Natl. Acad. Sci. USA *111*, E1291–E1299.

Tricoire, L., Pelkey, K.A., Erkkila, B.E., Jeffries, B.W., Yuan, X., and McBain, C.J. (2011). A blueprint for the spatiotemporal origins of mouse hippocampal interneuron diversity. J. Neurosci. *31*, 10948–10970.

Uemura, T., Lee, S.-J., Yasumura, M., Takeuchi, T., Yoshida, T., Ra, M., Taguchi, R., Sakimura, K., and Mishina, M. (2010). Trans-synaptic interaction of GluRdelta2 and Neurexin through Cbln1 mediates synapse formation in the cerebellum. Cell *141*, 1068–1079.

Ullrich, B., Ushkaryov, Y.A., and Südhof, T.C. (1995). Cartography of neurexins: more than 1000 isoforms generated by alternative splicing and expressed in distinct subsets of neurons. Neuron *14*, 497–507.

Ushkaryov, Y.A., and Südhof, T.C. (1993). Neurexin III alpha: extensive alternative splicing generates membrane-bound and soluble forms. Proc. Natl. Acad. Sci. USA *90*, 6410–6414.

Ushkaryov, Y.A., Petrenko, A.G., Geppert, M., and Südhof, T.C. (1992). Neurexins: synaptic cell surface proteins related to the alpha-latrotoxin receptor and laminin. Science *257*, 50–56.

Wall, N.R., De La Parra, M., Callaway, E.M., and Kreitzer, A.C. (2013). Differential innervation of direct- and indirect-pathway striatal projection neurons. Neuron *79*, 347–360.

Wickersham, I.R., Lyon, D.C., Barnard, R.J., Mori, T., Finke, S., Conzelmann, K.K., Young, J.A., and Callaway, E.M. (2007). Monosynaptic restriction of transsynaptic tracing from single, genetically targeted neurons. Neuron *53*, 639–647.

Yim, Y.S., Kwon, Y., Nam, J., Yoon, H.I., Lee, K., Kim, D.G., Kim, E., Kim, C.H., and Ko, J. (2013). Slitrks control excitatory and inhibitory synapse formation with LAR receptor protein tyrosine phosphatases. Proc. Natl. Acad. Sci. USA *110*, 4057–4062.

Zhao, Y., Marín, O., Hermesz, E., Powell, A., Flames, N., Palkovits, M., Rubenstein, J.L., and Westphal, H. (2003). The LIM-homeobox gene Lhx8 is required for the development of many cholinergic neurons in the mouse forebrain. Proc. Natl. Acad. Sci. USA *100*, 9005–9010.

Zipursky, S.L., and Sanes, J.R. (2010). Chemoaffinity revisited: dscams, protocadherins, and neural circuit assembly. Cell *143*, 343–353.